Tanzania Journal of Engineering and Technology 2025, **44**(1):289 - 304

Websites: https://ajol.org/tjet; https://tjet.udsm.ac.tz

ISSN 1821-536X (**print**); ISSN 2619-8789 (**electronic**)
https://doi.org/10.52339/tjet.v44i1.1160

Regular Research Manuscript

Improving Image Quality in Electrical Capacitance Tomography using OTSU Thresholding

Josiah Nombo
Department of Electronics and Telecommunications Engineering, College of Information and Communication Technologies, University of Dar es Salaam, Tanzania
Corresponding author: jpnomb@udsm.ac.tz; ORCID: 0000-0002-0020-6936

ABSTRACT

Electrical Capacitance Tomography (ECT) is an imaging technique used in industrial process monitoring, particularly for monitoring and measuring the composition of multiphase flows. Despite its widespread application, the commonly used Linear Back Projection (LBP) algorithm often produces low-quality images due to its limited ability to handle high permittivity contrasts and nonlinearities. This study investigates the use of Otsu thresholding as a post-processing technique to enhance ECT image quality. By maximizing inter-class variance in the image histogram, Otsu thresholding improves contrast, clarity, and structural definition, enabling more effective segmentation of oil and gas components in multiphase flows. The proposed Otsu-based reconstruction method, LBPU, was developed and evaluated alongside the standard LBP and entropy-based thresholding methods (LBPS and LBPT) using static experiments with an 8-electrode ECT measurement system. The qualitative visual assessment showed that the images created by LBPU had a clearer structure and were more visually similar to the reference images than the images generated by LBP, LBPS and LBPT for both the annular and stratified flows. Quantitatively, LBPU produced images with improved reconstruction accuracy by generating images with distribution error (DE) values below the 10% threshold and higher the correlation coefficient (CC) compared to other methods across the entire fraction of components. In terms of computational efficiency, the LBP method had the fastest processing time compared to other methods. The LBPU method required slightly more time than LBP but faster than LBPT and LBPS. These findings indicate that the LBPU method can be more suitable in online industrial monitoring applications demanding both speed and accuracy like those found in the oil and gas industry since it ensures a DE value threshold of 10% or less for proper multiphase flow visualization.

ARTICLE INFO
Submitted: Jan. 30, 2024
Revised: Apr. 20, 2025
Accepted: Apr. 29, 2025
Published: Apr. 2025

Keywords: *Electrical capacitance Tomography; inverse problem; image reconstruction; image segmentation thresholding; UTSU.*

INTRODUCTION

Electrical capacitance tomography (ECT) is an electronic imaging measurement system for monitoring and measuring internal parts of industrial processes (Guo et al., 2020; Liu & Yan, 2021; Shao, 2024) The system is widely used in hydrocarbon multiphase flow measurement and monitoring applications (Dimas et al., 2024; Hampel et al., 2022). Among the key requirements for these applications are fast scanning speed and reconstructions of high-quality images, as online applications require rapid adaptation to the dynamic changes in combustion and explosion processes within an enclosure (Nombo et al., 2021; Nyotoka et al., 2024). Despite its advantages and broad applications, ECT systems produce poor images with low spatial resolution, particularly when used in pipelines and pneumatic systems (Tiwari et al., 2022). This limits the applicability of ECT restoration methods to practical industrial systems (Deabes & Amin, 2020). On the other hand, ECT reconstruction presents inherent ambiguity which leads to various potential solutions. Moreover, ECT electronics experience non-zero leakage currents which lead to methods that create a non-linear correlation between capacitance and dielectric constant (Wang et al., 2020).

The Linear Back Projection (LBP) algorithm stands out as the optimal choice for online monitoring because of its simple design and efficient computational performance (Mwambela & Nombo, 2024; Zhu et al., 2019). However, it generates images of lower quality and fails to give the required resolution and accuracy for detailed quantitative analysis (Liu et al., 2022; Mwambela & Nombo, 2024). The algorithm's internal approximations cause defects in reconstructed images which lead to reduced quality. The pursuit of higher quality image reconstruction from these systems has motivated researchers to investigate novel reconstruction approaches. Researchers have proposed many different reconstruction algorithms over the last few decades to solve this challenge. Researchers have used filtering (Guo et al., 2019, 2020; Huang et al., 2022; X. Wu et al., 2013; Yang et al., 2023), data fitting (Nombo et al., 2014, 2015), and segmentation (Nombo et al., 2021), techniques for preprocessing images created with the LBP algorithm.

Thresholding stands out among segmentation-based preprocessing techniques as a powerful method for detecting and classifying image components (Dismas et al., 2024). Entropy-based thresholding techniques serve as an effective approach to image segmentation within ECT systems (Mwambela, 2018). Image processing through entropy-based thresholding methods like Shannon, Renyi, and Tsallis entropy achieves better noise reduction and image quality compared to LBP. These methods maintain information fidelity from original measurements through entropy optimization throughout the image creation process. However, the computational demands of these methods exceed available resources and fail to meet industrial online application requirements (Mwambela, 2018; Nombo et al., 2021).

Image quality enhancements resulted from the thresholding methods developed by Renyi and Tsallis which expanded entropy calculations and introduced flexible adjustments for various flow regimes and component distributions (Mwambela, 2018). This approach demonstrates enhanced performance across various conditions when compared to methods based on Shannon entropy. The complexity of these algorithms creates limitations for their use in real-world applications that have restricted computing resources. The global entropic thresholding methods face difficulties when dealing with the nonlinear nature of ECT imaging which becomes particularly challenging in conditions of low contrast or high background noise (Nombo et al., 2021).

Investigating alternative segmentation approaches that use statistical thresholds could help overcome current limitations and generate higher-quality images for industrial process monitoring. One promising technique is Otsu's thresholding (Otsu, 1979). The automatic thresholding technique of Otsu identifies the best threshold by maximizing the variation between foreground and background pixels in the histogram of an image (Katherine et al., 2021; Nyo et al., 2022). The implementation of Otsu's thresholding in ECT image reconstruction can result in more accurate component segmentation which enhances contrast and boundary definition (Al-Rahlawee & Rahebi, 2021; Zheng et al., 2022). The proposed method will improve the objectivity and efficacy of image reconstruction by producing high-quality images with significant computational efficiency.

In recent decades, Otsu thresholding has been widely used in pre- and post-processing in various applications. Studies have shown significant improvements in contrast, noise reduction and sharpness of the images compared to non-threshold methods (Al-Rahlawee & Rahebi, 2021; Katherine et al., 2021; Nyo et al., 2022; Tan et al., 2021). These advances improve visualization of the internal structure of the media and contribute to more accurate measurements, ultimately improving industrial processes and decision making based on quantitative data.

This study proposes a modified Otsu threshold method to improve the quality of the images produced by ECT systems. It covers the basics of ECT imaging, the challenges of reconstructing images and the theoretical basis for the Otsu threshold. In addition, new research and progress are presented in the application of the Otsu threshold for improving the image quality of ECT in a number of applications. Finally, possible further development of this method and its role as a non-invasive method of image acquisition is explored.

MATERIALS AND METHODS

ECT Measurement and Image Reconstruction Process

The electrical capacitance tomography (ECT) measurement procedure is shown in Figure 1. The process begins with the sensor array being carefully positioned around a vessel containing the material to be imaged. These sensors measure the permittivity distribution inside the container and capture important data about the internal structure of the material. They are responsible for learning the permittivity distribution inside the container. The sensors' energization to produce the necessary electrical signals that interact with the material is controlled by the excitation scheme. The controller is crucial at this point because it regulates the sensor array's operation and synchronizes the excitation and measurement processes to ensure accurate data collection. The measurement electronics then process the signals generated by the sensors, which are impacted by their interaction with the material, to produce raw capacitance data. (Chowdhury et al., 2022).

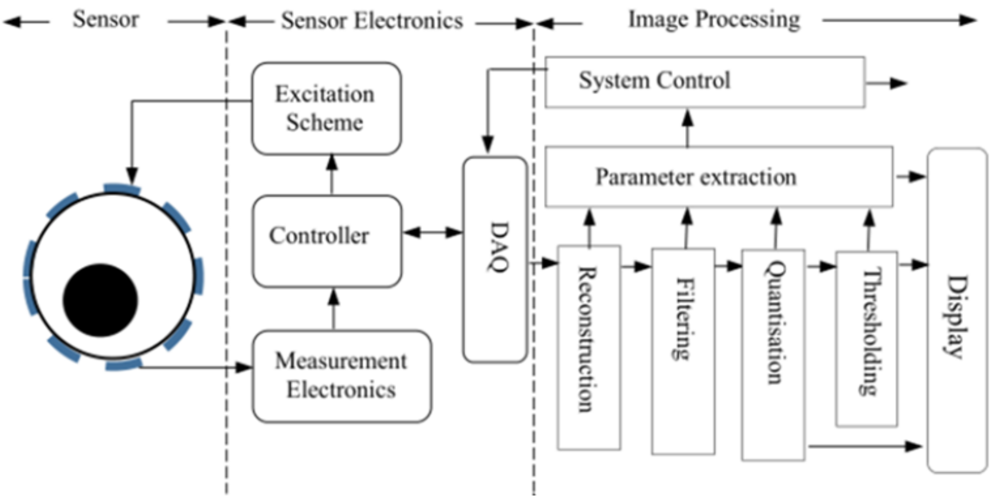

Figure 1: Description of the ECT Measurement Process (Mwambela, 2018).

The measured capacities are then recorded by the data acquisition (DAQ) system, which acts as a link between the image processing unit and the sensor electronics. Then, the system control unit takes over the image processing. This unit ensures the smooth coordination of entire the process from capacitance measurements to image display. Parameter extraction occurs during the image processing phase to extract relevant information from the raw capacitances and prepare it for image reconstruction (Chowdhury et al., 2022).

The process of reconstruction makes use of the extracted parameters to produce an image or of the internal structure of the material under observation (Xie et al., 2021). Filtering techniques are used to address any noise or artifacts that may have been present in the initial reconstruction. The quality of the image is enhanced by filtering, becoming sharper and more precise (Nombo et al., 2014). Following refinement, the image is quantized, a technique that breaks down continuous image data into discrete levels for easier analysis and interpretation. The image is subjected to thresholding after quantization in order to draw attention to important details, set them apart from the background, and enhance the image's focus and informational value(Nombo et al., 2021).

The improved and processed image is then sent to the display unit, for visualisation and further analysis. After going through several processing stages, the displayed image is now sharper and more useful for qualitative and quantitative analysis. It offers important information about the internal structure and behaviour of the material inside the vessel. This all-inclusive procedure, which includes everything from sensor data gathering to the final image display, captures the crucial phases of ECT and guarantees that the reconstructed images are of high quality, and helpful in a given industrial process.

ECT Reconstruction Problem

Image Reconstruction Problem in ECT

To reconstruct an ECT image, two computational problems need to be solved: forward and inverse (Huang et al., 2022). The Forward Problem, provided by

$$C = SG. \tag{1}$$

Equation (1) is a simplified model of the ECT system, it calculates the capacitance values from a given permittivity distribution (G) and field sensitivity matrix (S). From equation (1), G is a N×1-dimensional vector representing the image vector, N is the number of pixels in the image, C represents a M×1-dimensional vector indicating the normalized capacitance values, M is the number of the capacitance measurements, and S is a $M \times N$ field sensitivity matrix showing the effect of the permittivity distribution at each pixel on the capacitance between the electrodes reflects. This model relies on several simplifying assumptions: the relationship between capacitance and permittivity is linear, the system operates under quasi-static conditions, electrodes behave ideally, and the permittivity distribution is time-invariant during measurement. These assumptions make equation (1) computationally tractable, but they limit its ability to fully capture the nonlinear and dynamic nature of real ECT systems.

The inverse problem aims to compute G from the given capacitance data. However, in most cases, S is a non-square matrix with no direct inversion, hence make it difficult to obtain G from single step methods without addition maniputlations (Liu & Yan, 2021). This results in a number of reconstruction methods to solve the problem. Techniques for solving inverse problems can be divided into two groups: direct (single-step), where a single mathematical step is required to generate the result directly from the measured capacitance and sensitivity matrix; and iterative techniques, in which a set of objective functions is iteratively optimized until stable conditions are achieved.

One of the most popular single-step reconstruction techniques used in Electrical Capacitance Tomography (ECT) is Linear Back Projection (LBP). This approach uses a linear approximation to the measured capacitance data and the sensitivity matrix in order to directly compute the permittivity distribution. LBP is appealing because it is easy to use, computationally efficient, and appropriate for online imaging applications. Nonetheless, its capacity to resolve non-linearities and attain high spatial resolution in the reconstructed images is intrinsically constrained (Liu et al., 2022; Mwambela & Nombo, 2024). In LBP, the reconstructed image vector (G) is derived by a linear mapping of the capacitance vector (C) using the transpose of the sensitivity matrix (S), expressed as:

$$G = S^T C. \qquad (2)$$

while LBP demonstrates better performance when the permittivity difference between regions is low—owing to reduced non-linear interactions between pixels—its performance diminishes with higher permittivity differences. In such cases, the increased effect of non-linearities results in blurred or less accurate images (Mwambela & Nombo, 2024).

To improve the quality of images reconstructed by LBP, thresholding can be employed as a post-processing step. Thresholding enhances image clarity by suppressing noise and isolating significant permittivity variations, effectively mitigating the impact of non-linearities on the reconstructed images. This approach refines the permittivity distribution by setting predefined thresholds, thereby preserving critical features while discarding artifacts and ensuring more accurate and interpretable results (Mwambela, 2018).

Image Thresholding Methods

Thresholding is used to distinguish objects from background pixels in an image by determining the optimal set of threshold grey levels. These techniques can be divided into two categories: two-stage and multi-stage thresholding techniques. The two-stage thresholding method uses a single threshold T, while the multi-stage thresholding method uses two or more thresholds $T_1, T_2, \dots, T_n$. The challenge is to develop cost functions $J(T)$ that can be derived directly from the data, without the need for additional assumptions, to select appropriate thresholds to use as a basis for selection from the set of data provided.

Shannon proposed such cost functions based on the information theory concept of entropy. This is a concept that quantifies uncertainty in order to describe the information contained in an image (Graf, 2024). The entropy H for an image histogram $p(i)$ (normalized probability of each intensity level iii) is defined by equation (3)

$$\mathrm{H} = -\sum_{i}^{L} p(i) \log p(i), \qquad (3)$$

where L is the number of gray levels in the image and $p(i)$is the probability of occurrence of the gray level (i). The most information is gathered and the most uncertainty arises when there is no prior knowledge. The fundamental premise for the oil-gas tomogram scenario is that the grey levels of the tomogram's pixels can be used to identify oil and gas. The original grey level tomogram can be converted into a binary image by carefully choosing a thresholding grey level between the dominant values of the gas and oil intensities. This will cause the tomogram pixels linked to the gas and oil to take on values of zero and one, respectively. The entropy-based thresholding methods determine the optimal threshold grayscale values that produce maximum entropy (ME) by analysing the profile features of an image's grayscale histogram, which is used as a probability distribution. For a single threshold T, the image is divided into two classes: C_1 (background), consisting of grey levels $i = 1,2, \dots, T$ and C_2 (foreground), consisting of grey levels $i = T + 1, \dots, L$. The entropy for each class is computed by equation (4) and the total entropy H_{total} is then computed using equation (5) as.

$$\mathrm{H}(C_1) = -\sum_{i}^{T} p(i) \log p(i), \qquad (4)$$

$$\mathrm{H}(C_2) = -\sum_{i=T+1}^{L} p(i)\log p(i),$$

$$H_{total} = \mathrm{H}(C_1) + \mathrm{H}(C_2). \quad (5)$$

The ME criterion was used for image thresholding by Pun (1981), who introduced thresholding techniques that select the threshold T^* maximizing equation (6).

$$T^* = \arg\max_{T} H_{total} \quad (6)$$

Pun's work was further improved by Kapur et al. (1985), who developed the foundation of image thresholding using ME that improved and corrected Pun's theoretical work. Numerous thresholding techniques that address a range of issues and constraints, such as spatial data, entropy correlation, cross-entropy, and fuzzy logic applications, have been developed as a result of Kapur's work; a thorough examination can be found elsewhere in the literature (Bala & Kumar Sharma, 2023; Kowalski & Smyk, 2022; Rajinikanth et al., 2021; B. Wu et al., 2021).

Entropy-based methods have played a crucial role in image thresholding. However, the determination of entropy from reconstructed images shows different complexities. As a result, information-theoretical approaches, especially those based on Shannon's entropy concept, have aroused considerable interest. While Shannon's entropy offers a basic framework, it has certain restrictions.

To solve these problems, Renyi (1961) generalized Shannon entropy mathematically and created a family of parametric entropy measures. Renyi's entropy is defined by

$$H_q = \frac{1}{1-q}\log\left(\sum_{i}^{L} p(i)^q\right), \quad (7)$$

where $q > 0$ and $q \neq 1$ is a parameter that controls sensitivity to probability distributions. When $q \to 1$, Renyi entropy converges to Shannon entropy, demonstrating its versatility. Subsequently, Tsallis (1988) introduced a similar entropy framework based on statistical physics. Tsallis entropy is given by

$$H_q = \frac{1}{q-1}\left(1 - \sum_{i}^{L} p(i)^q .\right) \quad (8)$$

The Tsallis entropy converges to the Shannon entropy, similar to the Renyi entropy as $q \to 1$. Both frameworks include the parameter q, which reduces sensitivity to the shape of the probability distribution and allows explicit control over the trade-offs of the ME threshold. These measures highlight the flexibility and adaptability of entropy-based image thresholding methods. Entropy-based thresholding methods face challenges such as high computational requirements, poor performance with unclear histogram peaks, and sensitivity to parameters such as q (Abualigah et al., 2023; Amiriebrahimabadi et al., 2024). These weaknesses limit their efficiency and reliability in various applications.

Motivated from these advances, this study proposed the use OTSU thresholding in ECT, a widely used image segmentation technique in image processing industries. OTSU Threshold works by maximizing interclass variance to determine an optimal threshold and provides a robust and computational method for image analysis.

OTSU Thresholding for Improved ECT Image Reconstruction

Otsu's thresholding technique is used in this study to separate the foreground and background areas of the input image $G(k)$. This method minimizes the intra-class

variance of pixel intensities to determine the ideal threshold, guaranteeing that the variability within each segmented region is kept to a minimum. A bimodal distribution of pixel intensities is assumed by the method, with one peak representing the foreground and the other the background.
Given an image $G(k)$ with pixel intensities distributed between 0 and $L-1$, where L represents the maximum possible intensity, the histogram of the image is used to calculate the probability distribution of the pixel intensities. Let T be a possible threshold that divides the pixel intensity range into two classes: Class 1 consists of pixels with intensities below the threshold T and represent the background of the image. On the other hand, class 2 contains pixels with intensities greater than or equal to the threshold T, which represent the foreground of the image. The probabilities of each class are defined by

$$p_{c1(T)} = \sum_{i=0}^{T-1} p(i), \quad and \quad p_{c2(T)} = \sum_{i=T}^{L-1} p(i) \tag{9}$$

where $p(i)$, represent the probability of each intensity level (i). The mean intensities for the two classes are given by

$$\mu_1(T) = \frac{\sum_{i=0}^{T-1} i\, p(i)}{p_{c1}(T)}, and\ \mu_2(T) = \frac{\sum_{i=T}^{L-1} i\, p(i)}{p_{c2}(T)}. \tag{10}$$

The intra-class variance, which quantifies the spread of intensities within each class, is expressed as

$$\sigma_w^2(T) = p_{c1}(T) \cdot \sigma_1^2(T) + p_{c2}(T) \cdot \sigma_2^2(T) \tag{11}$$

where $\sigma_1^2(T)$and $\sigma_2^2(T)$ are the variances of Class 1 and Class 2, respectively. The goal of Otsu's method is to find the threshold T^* that minimizes the intra-class variance given by equation (12)

$$T^* = \arg\min_{T} \ \sigma_w^2(T). \tag{12}$$

This optimal threshold T^* ensures that the separation between the foreground and background regions is maximized in terms of intensity contrast. Once the threshold is identified, the segmented image $G(k)$ is computed using the following binary segmentation equation:

$$G(k) = \begin{pmatrix} 1 & if \ \ G(x) \geq T^* \\ 0 & if \ \ G(x) < T^* \end{pmatrix} \tag{13}$$

In this work, the Otsu thresholding algorithm was implemented using MATLAB, which provides a robust and efficient tool for automatic threshold selection. This approach ensures that the thresholding process is adaptive to the intensity distribution of each image, facilitating accurate separation of between oil and gas components. This method was chosen due to its simplicity, efficiency, and proven performance in applications where clear intensity-based separation between the foreground and background is required.

EXPERIMENTS SETUP AND EVALUATION CRITERIA

Experimental Setup

Experiments were conducted using an 8-electrode circular sensor ECT system (excitation waveform: 10Vpp, 300–500 kHz), with the sensing domain divided into 900 pixels using a 32 × 32 grid, to assess the effectiveness of the proposed method (Figure 2). Prior to the experiments, the sensor system was calibrated using air, oil and gas, to ensure measurement accuracy. Then multiple readings were taken to confirm consistency, including a noise test in air to verify signal stability. Perspex beads, arranged in both annular and stratified configurations, were used in static experiments and placed at various points within the sensing domain. The performance of the proposed method was examined across the full component fraction range using simulated capacitance data. All reconstruction methods were implemented in MATLAB and executed on a computer with an Intel Core i7-4510U CPU (2.0 GHz) and 8 GB of RAM.

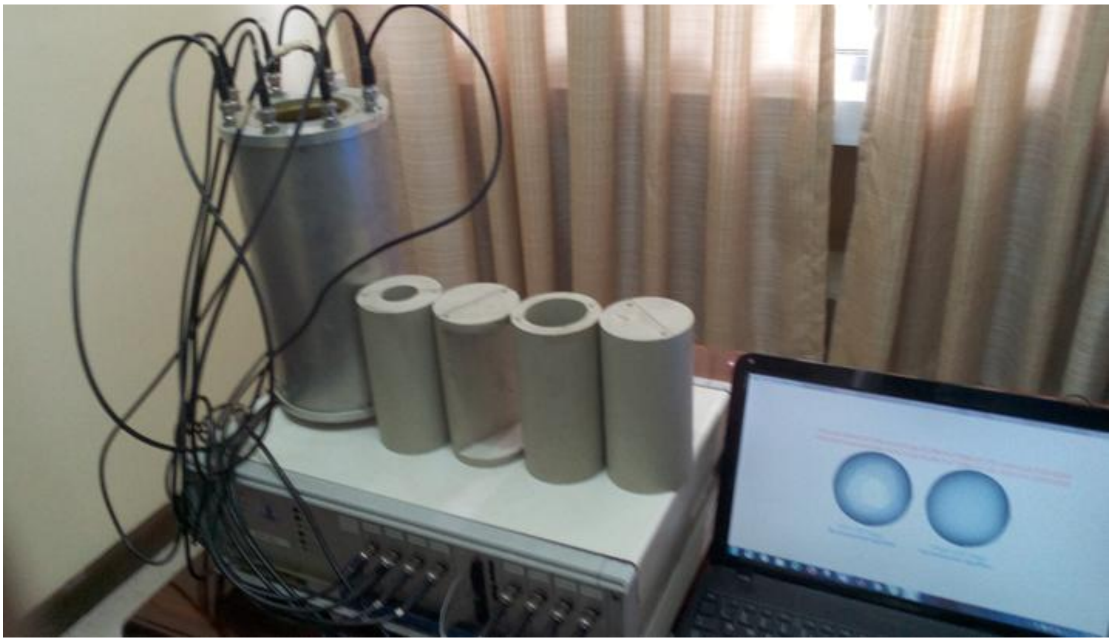

Figure 2: An 8-electrode sensor ECT system at the CoICT University of Dar es Salaam.

Evaluation Criteria

The performance assessment criteria for the proposed algorithm may be summarised on the basis of accuracy, reliability in different operating environments and applicability to the hydrocarbon industry (Hjertaker, 1998; Mwambela, 2018).

Accuracy refers to the ability of an algorithm to generate images that are spatially and volumetrically approximated to the original images. The comparative metrics used are the qualitative visual inspection as well as the quantitative distribution error (DE) and correlation coefficient (CC) as given by equations (14) and (15).

$$\mathrm{DE} = \frac{1}{N}\sum_{i=1}^{N} \left|G_i^{rec} - G_i^{ref}\right|, \qquad (14)$$

where G_i^{rec} and G_i^{ref} are, respectively, the reference and reconstructed image vectors for an image element i, and N represents the total number of pixels of the reconstructed image. Lower DE signals better results in reservoir management in oil industries, for example, the desired DE should be less or equal to 10% (Almutairi et al., 2020). The correlation coefficient (CC) between the reference image and the reconstructed image is given by

$$CC = \frac{\sum_{e=1}^{M} \left(\hat{G}(e) - \underline{\hat{G}}(e))(G(e) - \hat{G}(e)\right)}{\sqrt{\sum_{e=1}^{M} \left(\hat{G}(e) - \underline{\hat{G}}(e)\right)^2 \sum_{e=1}^{M} \left(\hat{G}(e) - \underline{\hat{G}}(e)\right)^2}} \qquad (15)$$

where, $\underline{G}$ and $\underline{\hat{G}}$ represent the average value of G and $\hat{G}$. The correlation coefficient represents the correlation between the true distribution and the reconstructed image. The closer the CC is to 1, the higher the quality. Robustness refers to the capability of the algorithm to consistently perform over full component volume fraction range and under various combination and conditions. Usability is the ability of the algorithm to be applied practically in the hydrocarbons industry to measure the component volume fraction of two-component multiphase flow (Table 2)(Mwambela, 2018).

An algorithm can be considered suitable for advanced ECT applications if it performs well in all three areas (accuracy, robustness and usability). This is particularly important in critical industries such as the hydrocarbon industry, where precision and reliability are crucial. For the purpose of experimentation and evaluation the algorithms are abbreviated as shown in Table 3.

Table 2: Accuracy requirements for a typical multiphase meter in hydrocarbons production over the full component volume fraction scale (Mwambela, 2018)

Oil industry Application	Desired Volumetric Accuracy
Reservoir management	$\sim \pm 10\%$ for all flow phases
Fiscal-custody transfer	$\sim \pm 2-5\%$ for all flow phases
	$\sim \pm 0.25\%$ for oil
Fiscal-Taxation/royalty	$\sim \pm 2\%$ for water
	$\sim \pm 1\%$ for gas

Table 3: Algorithms evaluated and associated abbreviations

Algorithms	Description
LBP	Linear Back Projection
LBPS	Thresholding algorithm using Shannon entropy
LPBT	Thresholding algorithm using Tsallis entropy
LBPU	Thresholding algorithm UTSU segmentation

RESULTS AND DISCUSSION

Figure 3 shows images reconstructed using LBP, LBPS, LBPT, and LBPU methods for annular, bubble, and stratified flow types along with their respective reference images. Each row represents a different flow type and each column (except the flow type and reference image columns) represents images reconstructed from different methods. The LBP method generates poor images with blurred boundaries. Images generated by LBPS method have preserved overall shape but introduces a pixelated texture. LBPT produces images with sharp and clear boundaries, but it diminishes the middle part reconstructed image, especially for annular flows. The LBPU successfully creates high quality images which resemble respective reference images while maintaining the clarity and structural integrity. The generated images by LPBU are of higher resolution and clear definition of boundaries. This superior performance of LBPU suggests its potential as an effective ECT reconstruction method for automatic industrial process control and monitoring applications.

To better evaluate the efficacy of the proposed approach, the evaluation was extended to include a quantitative assessment over the full component fraction range for annular and stratified flows. Figure 4 shows the distribution error (DE)-based quantitative performance of LBP, LBPS, LBPT, and LBPU for annular flows across the full component fraction range. Poor performance was observed by the standard LBP method which consistently generate images with high DE values, which are above the 10% threshold across the majority of Reference Gas Fraction (RGF) percentages. LBPS and LBPT showed intermediate performance, with DE values varying around the threshold of 10%; Their DE values remained below 10% at midrange RGF but exceeded at lower and higher percentages. On the other hand, LBPU demonstrated the most stable and reliable performance, keeping DE values below 10% across the entire range of RGF percentages, making it a suitable choice for applications requiring high accuracy.

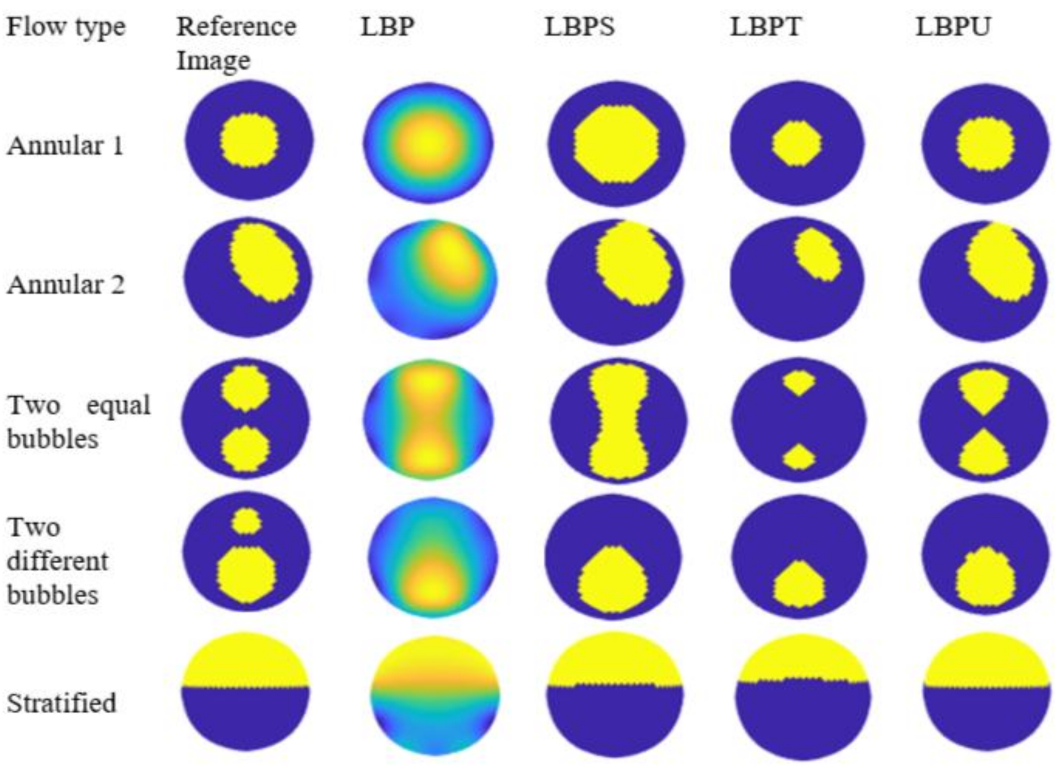

Figure 3: Qualitative visual comparison of images reconstructed by LBP, LBPS, LBPT and LBPU for selected samples of annular and stratified flow.

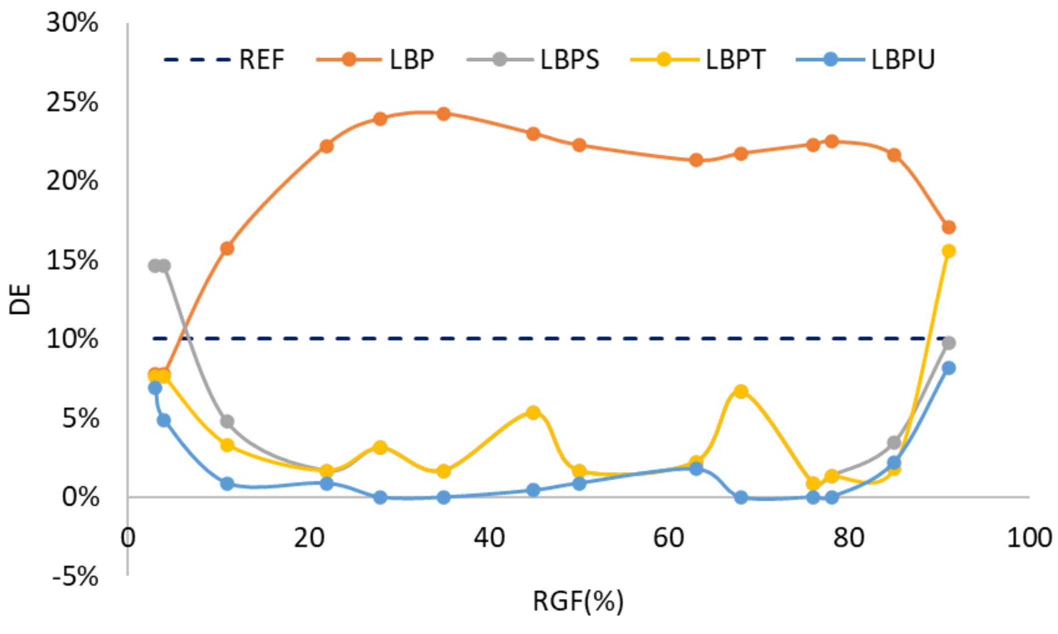

Figure 4: The distribution error (DE) performance of LBP, LBPS, LBPT, and LBPU over full component fraction range for annular flow.

For stratified flow, the quantitative assessment of LBP, LBPS, LBPT, and LBPU across the full component fraction range is displayed in Figure 5. The standard LBP method showed consistently high DE values that are above the 10% threshold across the entire RGF range, indicating poor performance. This is mainly because LBP struggles to resolve sharp horizontal interfaces since it relies on a basic linear approximation, which limits its effectiveness—particularly in stratified flow conditions where clear phase separation is critical. LBPS and LBPT performed moderately, with DE values consistently remaining below the threshold of 10%. LBPU, on the other hand, kept DE values well below 10% throughout the whole RGF range, exhibiting the most reliable performance. Conversely, LBPU demonstrated the best performance by maintaining DE values well below 10% across the entire RGF range. This suggests its usefulness for oil industry application that need low DE as stipulated in Figure 5.

Figure 6 shows correlation coefficient (CC) performance for four reconstruction methods - LBP, LBP, LPT, and LPU - over the entire range of relative gas fractions (RGF) in the annular flow. LBPU consistently gives better results compared to other methods by maintained CC values near 1.0, indicating higher accuracy and robustness in ECT image reconstruction. Compared to LBPU, LBP and LBPS showed weaker performance, especially at lower gas fractions, with a slight improvement in the mid-range of the RGF and a slight decrease at higher values. In particular, the LBP and the LBPS performed better than the mid-range RGF but were still inferior to the LBPU.

Figure 7 presents the correlation coefficient (CC) performance of four reconstruction methods—LBP, LBPS, LBPT, and LBPU—across a full range of relative gas fractions (RGF%) in stratified flow. LBPU gives the highest CC values throughout the entire range, consistently near or above 0.95, indicating its high ability to accurately reconstruct phase distributions. In contrast, LBP shows lower performance, especially at low RGF values (below 20%), where CC drops to around 0.75. Both LBPS and LBPT improve upon LBP, with LBPT slightly outperforming LBPS at most points. The performance gap is mostly seen at the extremes of the RGF range, where LBPU maintains high accuracy while others decline. These results confirm that LBPU is more reliable under variable flow conditions, making it better suited for accurate imaging in multiphase flows such as oil and gas.

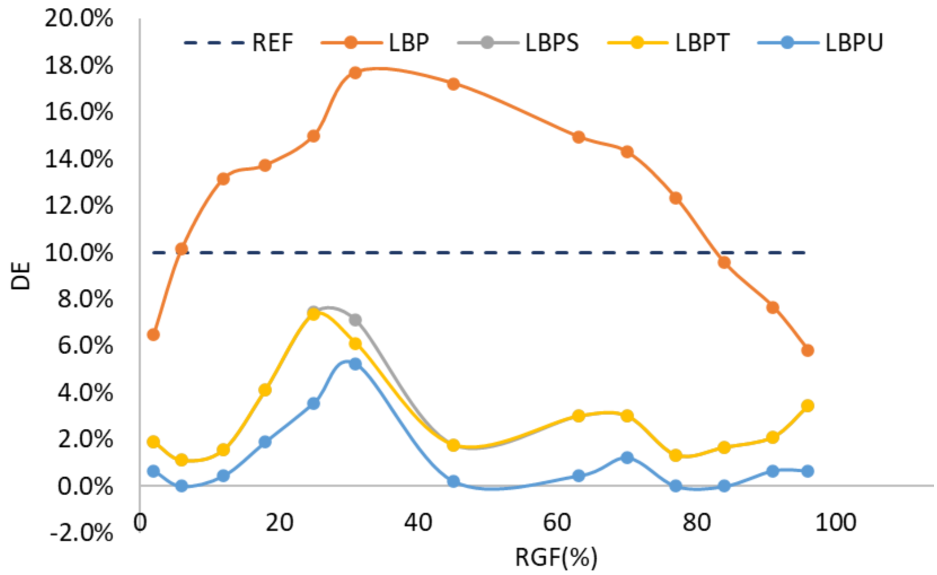

Figure 5: The distribution error (DE) performance of LBP, LBPS, LBPT, and LBPU over full component fraction range for stratified flow.

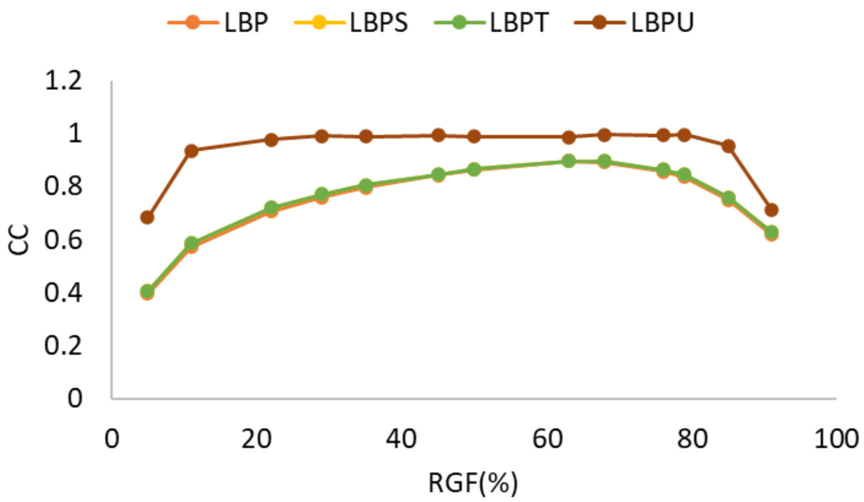

Figure 6: The correlation coefficient (CC) performance of LBP, LBPS, LBPT, and LBPU over full component fraction range for annular flow.

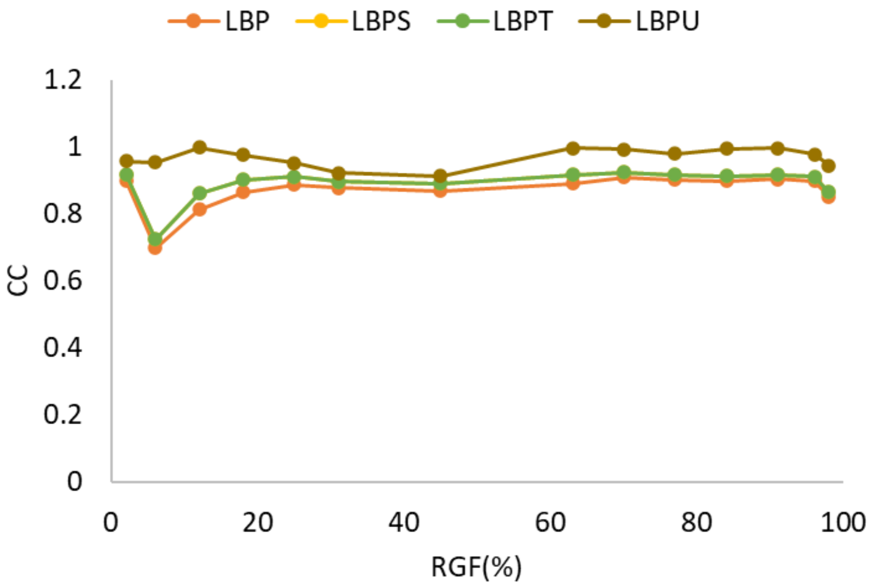

Figure 7: The correlation coefficient (CC) performance of LBP, LBPS, LBPT, and LBPU over full component fraction range for stratified flow.

The relative execution times of the four algorithms (LBP, LBPS, LBPT, and LBPU) under annular and stratified flow conditions are shown in Figure 8, along with the average execution time for all four. With 0.16 seconds for annular flow, 0.17 seconds for stratified flow, and a similar average of 0.17 seconds, the results show that LBP continuously obtained the quickest execution time. As a result, of the four approaches, LBP has the highest computational efficiency. With an overall average of 0.26 seconds, LBPU also showed comparatively short execution times, especially in annular flow (0.23 seconds) and stratified flow (0.29 seconds). LBPU was still much faster than LBPT and LBPS, despite being a little more computationally demanding than LBP. On the other hand, LBPT had the longest execution time of any flow type, averaging 0.58 seconds overall and reaching a peak of 0.74 seconds in stratified flow. With an average of 0.43 seconds, 0.36 seconds for annular flow, and 0.50 seconds for stratified flow, LBPS also required a moderate amount of computation time. All things considered, these results show a definite trade-off between computational complexity and possible performance, with LBP and LBPU providing faster processing appropriate for online applications and LBPT, despite its longer execution time, possibly providing additional accuracy or robustness benefits that outweigh its computational expense.

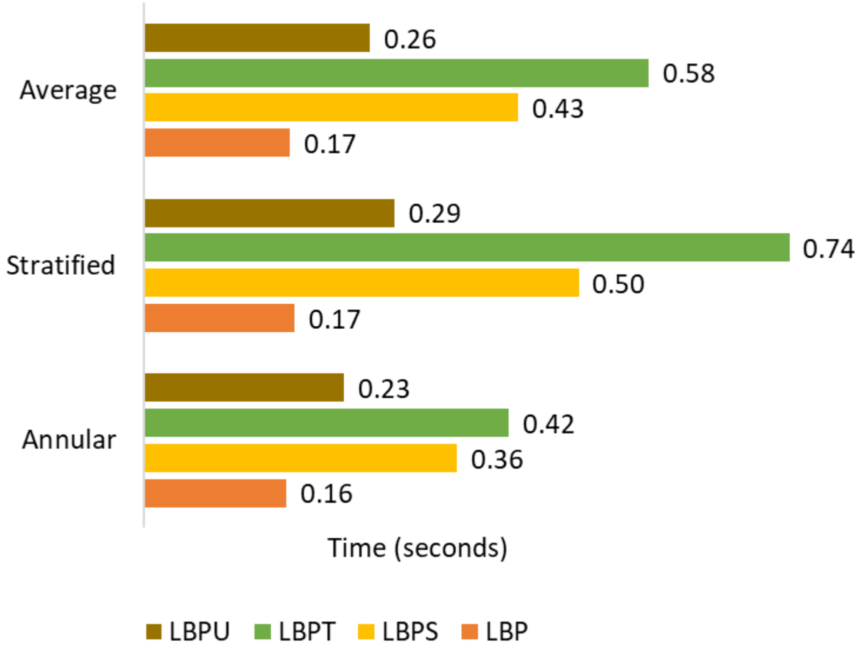

Figure 8: The average execution time for LBP, LBPS, LBPT, and LBPU.

The results of this study indicate that the LBPU approach has a lot of potential for online flow monitoring and industrial process control. Maintaining operational efficiency, equipment reliability, and safety in sectors like multiphase transport, chemical processing, and oil and gas production depends on precise internal flow pattern visualization. LBPU demonstrated consistent performance across a full range of flow conditions and component fractions. Its ability to accurately reconstruct the underlying flow structure was further demonstrated by the fact that it obtained the highest correlation coefficient (CC) values out of all the methods assessed. LBPU showed a high degree of computational efficiency in addition to accuracy. It was not the fastest method, but it was still feasible for online applications given its execution time. Because of its ability to balance speed and performance, it is a good choice for settings where image fidelity and timely processing are crucial. Preserving internal characteristics and boundary clarity is another strength of LBPU, which improves the dependability of flow interpretation and facilitates better operational decision-making. The ability to accurately and in real time monitor complex flows, like annular and stratified patterns, is essential in practice, especially in the oil and gas industry, for production optimization, early flow problem detection, and averting expensive failures like pipeline blockages. According to these findings the accuracy, responsiveness, and general safety of multiphase flow monitoring systems can all be enhanced with implementation of LBPU.

CONCLUSION

This study examined how to improve image quality in Electrical Capacitance Tomography (ECT) systems used for industrial process monitoring by implementing Otsu's thresholding method. It addressed a major drawback of the widely used Linear Back Projection (LBP) technique, which usually results in low-resolution images with blurred borders despite its speed. Clearer and more detailed images are produced by Otsu's method, which maximizes inter-class variance and enables more accurate segmentation of image regions. This is a significant benefit for efficient monitoring and control in oil and gas operations. In this study, four reconstruction techniques were compared: LBP, LBPS, LBPT, and the proposed LBPU. The results showed that LBPU delivers the most reliable performance. It regularly generated excellent images with distribution error (DE) values less than 10%, which is within the allowable range for hydrocarbon monitoring. Additionally, the best correlation coefficient (CC) values were obtained by LBPU, indicating a high degree of agreement between the reconstructed and the reference images. The execution time was well within the range appropriate for online applications, providing a useful balance between computational efficiency and image fidelity, even though it took a little longer to process than LBP. LBPU was superior in accuracy and consistency, while entropy-based techniques such as LBPS and LBPT yielded only modest gains. Additionally, the study emphasizes Otsu's thresholding's adaptability and simplicity of use, confirming its appropriateness for industrial ECT applications where precision, dependability, and ease of use are crucial. Even though the current method successfully enhances image quality and segmentation, future studies could investigate hybrid approaches or more sophisticated algorithms to further improve performance, especially in flow conditions that are noisy or highly dynamic. Overall, the linear back projection reconstruction method in conjunction with Otsu's thresholding provides a reliable and effective online multiphase flow monitoring solution for the hydrocarbon sector.

REFERENCES

Abualigah, L., Almotairi, K. H., & Elaziz, M. A. (2023). Multilevel thresholding image segmentation using meta-heuristic optimization algorithms: comparative analysis, open challenges and new trends. *Applied Intelligence*, **53**(10), 11654–11704. doi:10.1007/S10489-022-04064-4/METRICS

Almutairi, Z., Al-Alweet, F. M., Alghamdi, Y. A., Almisned, O. A., & Alothman, O. Y. (2020). Investigating the Characteristics of Two-Phase Flow Using Electrical Capacitance Tomography (ECT) for Three Pipe Orientations. *Processes*, **8**(1), 51. doi:10.3390/PR8010051

Al-Rahlawee, A. T. H., & Rahebi, J. (2021). Multilevel thresholding of images with improved Otsu thresholding by black widow optimization algorithm. *Multimedia Tools and Applications* **80**(18), 28217–28243. doi:10.1007/S11042-021-10860-W

Amiriebrahimabadi, M., Rouhi, Z., & Mansouri, N. (2024). A Comprehensive Survey of Multi-Level Thresholding Segmentation Methods for Image Processing. *Archives of Computational Methods in Engineering* **31**(6), 3647–3697. doi:10.1007/S11831-024-10093-8

Bala, A., & Kumar Sharma, A. (2023). A Review on Various Thresholding Technique for Image Segmentation. *International Journal of Advances in Engineering and Management (IJAEM)*, **5**(7), 380–390. doi:10.35629/5252-0507380390

Chowdhury, S. M., Marashdeh, Q., Teixeira, F. L., & Fan, L. S. (2022). Electrical Capacitance Tomography. *Industrial Tomography: Systems and Applications, Second Edition*, 3–29. doi:10.1016/B978-0-12-823015-2.00002-9

Deabes, W., & Amin, H. H. (2020). Image reconstruction algorithm based on PSO-tuned fuzzy inference system for electrical capacitance tomography. *IEEE Access*, **8**, 191875–191887. doi:10.1109/ACCESS.2020.3033185

Dimas, C., Alimisis, V., Uzunoglu, N., & Sotiriadis, P. (2024). Advances in Electrical Impedance Tomography Inverse Problem Solution Methods: From Traditional Regularization to Deep Learning. *IEEE Access*. doi:10.1109/ACCESS.2024.3382939

Dismas, J., Ally, N., Nombo, J., Mwambela, A., & Maiseli, B. (2024). Perona-Malik Diffusion-Driven Regularization for Image Resolution Enhancement in Electrical Capacitance Tomography. *Tanzania Journal of Engineering and*

Technology, **43**(2), 139–149. doi:10.52339/tjet.v43i2.997

Graf, H. (2024). Claude Shannon and Warren Weaver (1949) The Mathematical Theory of Communication. In *Classics in Media Theory* (1st Edition, pp. 70–83). Taylor and Francis. doi:10.4324/9781003432272-6

Guo, Q., Li, X., Hou, B., Mariethoz, G., Ye, M., Yang, W., & Liu, Z. (2020). A Novel Image Reconstruction Strategy for ECT: Combining Two Algorithms with a Graph Cut Method. *IEEE Transactions on Instrumentation and Measurement*, **69**(3), 804–814. doi:10.1109/TIM.2019.2905282

Guo, Q., Ye, M., Yang, W., & Liu, Z. (2019). A machine learning approach for electrical capacitance tomography measurement of gas–solid fluidized beds. *AIChE Journal*, **65**(6), e16601. doi:10.1002/aic.16583

Hampel, U., Babout, L., Banasiak, R., Schleicher, E., Soleimani, M., Wondrak, T., Vauhkonen, M., Lähivaara, T., Tan, C., Hoyle, B., & Penn, A. (2022). A Review on Fast Tomographic Imaging Techniques and Their Potential Application in Industrial Process Control. *Sensors*, **22**(6), 2309. doi:10.3390/S22062309

Hjertaker, B. T. (1998). Static characterization of a dual sensor flow imaging system. *Flow Measurement and Instrumentation*, **9**(3), 183–191. doi:10.1016/S0955-5986(98)00018-1

Huang, G., Sun, J., Lu, W., Peng, H., & Wang, J. (2022). ECT Image Reconstruction Method Based on Multi-Exponential Feature Extraction. *IEEE Transactions on Instrumentation and Measurement*, **71**. doi:10.1109/TIM.2021.3132829

Kapur, J., Sahoo, P., & Wong, A. (1985). A new method for gray-level picture thresholding using the entropy of the histogram. *Computer Vision, Graphics, and Image Processing*, **29**, 273–285. https://doi.org/10.1016/0734-189X(85)90125-2

Katherine, Rulaningtyas, R., & Ain, K. (2021). CT scan image segmentation based on hounsfield unit values using Otsu thresholding method. *Journal of Physics: Conference Series*, **1816**(1), 012080. doi:10.1088/1742-6596/1816/1/012080

Kowalski, P., & Smyk, R. (2022). Comparison of thresholding algorithms for automatic overhead line detection procedure. *Przegląd Elektrotechniczny*, **98**(3), 149–155. doi:10.15199/48.2022.03.34

Liu, X., & Yan, C. (2021). Application of improved Landweber algorithm for ECT image reconstruction. *Proceedings - 2021 17th International Conference on Computational Intelligence and Security, CIS 2021*, 294–298. doi:10.1109/CIS54983.2021.00068

Liu, X., Yue, S., & Ren, H. (2022). A λ-level partition-based linear back projection algorithm to electrical resistance tomography. *Conference Record - IEEE Instrumentation and Measurement Technology Conference*. doi:10.1109/I2MTC48687.2022.9806584

Mwambela, A. (2018). Comparative Performance Evaluation of Entropic Thresholding Algorithms Based on Shannon, Renyi and Tsallis Entropy Definitions for Electrical Capacitance Tomography Measurement Systems. *International J. Intelligent Systems and Applications*, 10(April), 41–49. doi:10.5815/ijisa.2018.04.05

Mwambela, A., & Nombo, J. (2024). Image Reconstruction Method Based on Iterative Linear Back Projection and Logistic Forward Solver for Electrical Capacitance Tomography Measurement System. *Tanzania Journal of Science*, **50**(2), 347–358. doi:10.4314/TJS.V50I2.14

Nombo, J., Mwambela, A., & Kisangiri, M. (2021). Analysis and Performance Evaluation of Entropic Thresholding Image Processing Techniques for Electrical Capacitance Tomography Measurement System. *Tanzania Journal of Science*, **47**(3), 928–942. doi:10.4314/tjs.v47i3.

Nombo, J., Mwambela, A., & Kisangiri, M. (2014). A Grey Level Fitting Mechanism based on Gompertz Function for Two Phase Flow Imaging using Electrical Capacitance Tomography Measurement. *International Journal of Computer Applications*, **101**(8), 7–12. doi: 10.5120/17705-8704

Nombo, J., Mwambela, A., & Michael, K. (2015). Performance Analysis of Grey Level Fitting Mechanism based Gompertz Function for Image Reconstruction Algorithms in Electrical Capacitance Tomography Measurement System. *International Journal of*

Computer Applications, **109**(15), 9–4. https://dspace.nm-aist.ac.tz/handle/20.500.12479/439

Nyo, M. T., Mebarek-Oudina, F., Hlaing, S. S., & Khan, N. A. (2022). Otsu's thresholding technique for MRI image brain tumor segmentation. *Multimedia Tools and Applications*, **81**(30), 43837–43849. doi:10.1007/S11042-022-13215-1/METRICS

Nyotoka, G., Ally, N., & Nombo, J. (2024). Diffusion-Steered Algorithm for Improving Quality of Images Generated by Electrical Capacitance Tomography Measurement System. *Tanzania Journal of Science*, **50**(2), 387–396. doi:10.4314/TJS.V50I2.17

Otsu, N. (1979). Threshold Selection Method from Gray-Level Histograms. *IEEE Trans Syst Man Cybern*, *SMC-9*(1), 62–66. doi:10.1109/TSMC.1979.4310076

Pun, T. (1981). Entropic thresholding, a new approach. *Computer Graphics and Image Processing*, **16**(3), 210–239. http://www.sciencedirect.com/science/article/pii/0146664X81900381

Rajinikanth, V., Kadry, S., Crespo, R. G., & Verdú, E. (2021). A Study on RGB Image Multi-Thresholding using Kapur/Tsallis Entropy and Moth-Flame Algorithm. *International Journal of Interactive Multimedia and Artificial Intelligence*, **7**(2), 163–171. doi:10.9781/IJIMAI.2021.11.008

Renyi, A. (1961). On measures of entropy and information. *Proceedings of the 4th Berkeley Symposium on Mathematical Statistics and Probability*, **1**, 547–561.

Shao, Y. (2024). Exposition and implementation of linear equation system reconstruction method in electromagnetic wave CT imaging. doi:10.1117/12.3021265, **13063**, 107–114. https://doi.org/10.1117/12.3021265

Tan, Z. Y., Basah, S. N., Yazid, H., & Safar, M. J. A. (2021). Performance analysis of Otsu thresholding for sign language segmentation. *Multimedia Tools and Applications*, **80**(14), 21499–21520. doi:10.1007/S11042-021-10688-4/METRICS

Tiwari, V. K., Meribout, M., Khezzar, L., Alhammadi, K., & Tarek, M. (2022). Electrical Tomography Hardware Systems for Real-time Applications: A Review. *IEEE Access*. doi:10.1109/ACCESS.2022.3203584

Tsallis, C. (1988). Possible generalization of Boltzmann-Gibbs statistics. *Journal of Statistical Physics*, **52**(1–2), 479–487. doi:10.1007/BF01016429/METRICS

Wang, S., Sun, X., Xu, C., Bao, J., Peng, C., & Tang, Z. (2020). Investigation of a circulating turbulent fluidized bed with a fractal gas distributor by electrostatic-immune electrical capacitance tomography. *Powder Technology*, **361**, 562–570. doi:10.1016/J.POWTEC.2019.11.077

Wu, B., Zhu, L., Cao, J., & Wang, J. (2021). A Hybrid Preaching Optimization Algorithm Based on Kapur Entropy for Multilevel Thresholding Color Image Segmentation. *Entropy*, **23**(12), 1599. doi:10.3390/E23121599

Wu, X., Huang, G., Wang, J., & Xu, C. (2013). Image reconstruction method of electrical capacitance tomography based on compressed sensing principle. *Measurement Science and Technology*, **24**(7), 075401(7pp). doi:10.1088/0957-0233/24/7/075401

Xie, H., Xia, T., Tian, Z., Zheng, X., & Zhang, X. (2021). A least squares support vector regression coupled linear reconstruction algorithm for ECT. *Flow Measurement and Instrumentation*, **77**, 101874. doi:10.1016/J.FLOWMEASINST.2020.101874

Yang, Y., Liu, J., & Liu, G. (2023). Image reconstruction for ECT based on high-order approximate sensitivity matrix. *Measurement Science and Technology*, **34**(9), 095402. doi:10.1088/1361-6501/ACDDD8

Zheng, J., Gao, Y., Zhang, H., Lei, Y., & Zhang, J. (2022). OTSU Multi-Threshold Image Segmentation Based on Improved Particle Swarm Algorithm. *Applied Sciences* **12**(22), 11514. doi:10.3390/APP122211514

Zhu, H., Sun, J., Xu, L., & Sun, S. (2019). Improving image reconstruction in electrical capacitance tomography based on deep learning. *2019 IEEE International Conference on Imaging Systems and Techniques (IST)*, 1–5. doi:10.1109/IST48021.2019.9010087.